

Msanii: High Fidelity Music Synthesis on a Shoestring Budget

Work-in-Progress (WiP)

Kinyugo Maina

Independent Researcher

kinyugomaina@gmail.com

January 18, 2023

Abstract

In this paper, we present Msanii, a novel diffusion-based model for synthesizing long-context, high-fidelity music efficiently. Our model combines the expressiveness of mel spectrograms, the generative capabilities of diffusion models, and the vocoding capabilities of neural vocoders. We demonstrate the effectiveness of Msanii by synthesizing tens of seconds (*190 seconds*) of *stereo* music at high sample rates (*44.1 kHz*) without the use of concatenative synthesis, cascading architectures, or compression techniques. To the best of our knowledge, this is the first work to successfully employ a diffusion-based model for synthesizing such long music samples at high sample rates. Our demo can be found [here](#) and our code [here](#).

1 Introduction

Music is a universal language that elicits emotions and connects people from diverse cultures, and is an integral part of society. For decades, researchers have been investigating whether computers can capture the creative process behind music creation and the potential implications for music and artificial intelligence.

In recent years, the field of generative modeling has seen significant growth with various techniques, including generative adversarial networks (GANs) [Goodfellow et al. \(2020\)](#), variational autoencoders (VAEs) [Kingma and Welling \(2013\)](#), normalizing flows [Rezende and Mohamed \(2015\)](#), autoregressive models [Dhariwal et al. \(2020\)](#), and diffusion models [Sohl-Dickstein et al. \(2015\)](#); [Ho et al. \(2020\)](#); [Kingma et al. \(2021\)](#), driving progress in various fields. These techniques have achieved human-level performance in tasks such as image generation [Rombach et al. \(2022\)](#); [Karras et al. \(2020\)](#); [Dhariwal and Nichol \(2021\)](#); [Saharia et al. \(2022\)](#); [Ramesh et al. \(2022\)](#), speech generation [Kong et al. \(2020\)](#); [Shen et al. \(2017\)](#), and text generation [Brown et al. \(2020\)](#); [Scao et al. \(2022\)](#), as well

as progressed music generation [Dhariwal et al. \(2020\)](#); [Rouard and Hadjeres \(2021\)](#); [Engel et al. \(2019\)](#); [Marafioti et al. \(2019\)](#) and other areas.

However, efficient high-fidelity music synthesis remains a challenging task in machine learning due to the high dimensionality of audio signals, which makes it difficult for models to learn the long-range structure of music [Dhariwal et al. \(2020\)](#); [Dieleman et al. \(2018\)](#). To address this issue, it is common to learn a lower-dimensional representation of the audio signal, which can reduce computational complexity and allow models to better capture the salient features of music related to fidelity [Dhariwal et al. \(2020\)](#); [Dieleman et al. \(2018\)](#). As an alternative to learning a lower-dimensional representation, Time-Frequency (TF) representations, such as mel spectrograms, provide a powerful and intuitive way to represent features in audio signals. Mel spectrograms, which are a type of TF feature, have been widely used in various applications, including natural language processing [Shen et al. \(2017\)](#), voice conversion [Hwang et al. \(2020\)](#), and singing voice synthesis [Liu et al. \(2022a\)](#). They have also been applied success-

fully to music synthesis Engel et al. (2019); Marafioti et al. (2019); Pasini and Schlüter (2022). Mel spectrograms are particularly appealing for music synthesis due to their low resolution, which allows them to capture important musical characteristics while minimizing computational complexity.

Autoregressive models and GANs are popular choices for music synthesis, but they each have their own challenges. Autoregressive models, which have been widely used in the raw waveform domain Dhariwal et al. (2020); Dieleman et al. (2018), are often slow at inference. GANs, which have frequently been employed for music synthesis using TF representations Engel et al. (2019); Marafioti et al. (2019); Pasini and Schlüter (2022), can suffer from unstable training and the adversarial training of multiple networks, leads to low sample diversity, in addition to being computationally expensive. In contrast, diffusion-based models offer fast inference compared to autoregressive models, a simple training procedure, and have recently outperformed GANs in terms of quality Dhariwal and Nichol (2021). This makes diffusion-based models an attractive choice for music synthesis.

In this paper, we propose a novel approach for music synthesis using mel spectrograms that leverages the benefits of diffusion-based modeling. By combining the expressiveness of mel spectrograms with our novel U-Net architecture and diffusion models, we are able to synthesize minutes of high-fidelity music at a high sample rate. Our method represents a significant advance in the field of music synthesis, as it generates long samples of high-quality music without relying on concatenative synthesis, cascading architectures, or compression techniques. Additionally, we show that our model, Msanii, can be used to solve other audio tasks, such as audio inpainting and style transfer, without the need for retraining.

The main contributions of this paper are:

- We introduce Msanii, a novel diffusion-based model for long-context, high-fidelity music synthesis in the mel spectrogram domain. To the best of our knowledge, this is the first work to successfully employ a diffusion-based model for synthesis of minutes of audio at high sample rates (44.1 kHz) in the TF domain.
- We demonstrate the effectiveness of Msanii by synthesizing tens of seconds (190 seconds) of stereo music at a high sample rate (44.1 kHz).
- We show that Msanii can be used to solve other audio tasks, such as interpolation, style transfer,

inpainting and outpainting, without the need for retraining.

The rest of the paper is organized as follows: in Section 2 we review related work in music synthesis and diffusion-based models. In Section 3 we describe our proposed method, including the architecture and training of Msanii. In Section 4 we present our experimental setup. In Section 5 we present our results. In Section 6 we discuss potential future work. And Finally, in Section 7 we summarize our contributions.

DISCLAIMER: This paper is a work in progress and has not been finalized. The results presented in this paper are subject to change and should not be considered final.

2 Background

The high dimensionality of audio signals presents a significant challenge for music synthesis in the raw waveform domain. To accurately represent an audio sample, it is necessary to discretize the continuous signal into a large number of samples, which requires a high sample rate (thousands of samples per second). For music at CD quality, this sample rate is typically 44.1 kHz. This means that a ~ 3 minute long audio sample will consist of approximately ~ 8 million samples. This complexity increases with the number of channels, as the total number of samples T becomes $T = \text{duration} \times \text{sample rate} \times \text{channels}$.

The computational demands of synthesizing long audio samples are further compounded by the need to capture a wide range of musical structures, such as timbre, harmony, and melody, as well as to ensure global coherence in terms of form and texture. To address these challenges, it is common to use a lower-dimensional representation of the audio signal that captures important musical features while minimizing computational complexity. Additionally, it is necessary to employ an expressive but efficient generative model.

2.1 Mel Spectrograms

To address the computational complexity of our task, we propose the use of a lower-dimensional yet expressive representation of audio: Mel Spectrograms. Mel spectrograms are a popular representation of audio used in tasks such as speech synthesis Shen et al. (2017), voice conversion Hwang et al. (2020), and music synthesis Vasquez and Lewis (2019). They are derived from the magnitude spectrogram of the Short-Time Fourier Transform (STFT) and encode frequency in a way that is more perceptually relevant to human hearing. However, the conversion from raw

audio to mel spectrograms is not perfectly invertible due to the loss of phase information in the magnitude STFT spectrogram.

To reconstruct audio from mel spectrograms, neural vocoders such as MelGAN [Kumar et al. \(2019\)](#), ISTFTNet [Kaneko et al. \(2022\)](#), MCNN [Arik et al. \(2018\)](#) and Phase Gradient [Di Giorgi et al. \(2022\)](#) have been developed to approximate both the magnitude and phase from the mel spectrogram. However, designing a vocoder that reconstructs both the magnitude and phase while remaining lightweight can be challenging. As an alternative, we propose reconstructing only the magnitude spectrogram and approximating the phase using traditional methods. This approach has been demonstrated in previous work such as Adversarial Audio Synthesis [Marafioti et al. \(2019\)](#) and MelNet [Vasquez and Lewis \(2019\)](#). In particular, we use the Griffin-Lim algorithm [Griffin and Lim \(1984\)](#); [Perraudin et al. \(2013\)](#).

To reconstruct the magnitude spectrogram, we use a combination of the Spectral Convergence Loss and Log-Magnitude Loss. The Spectral Convergence Loss is defined as:

$$\frac{\| |STFT(s)| - |STFT(\hat{s})| \|_F}{\| |STFT(s)| \|_F} \quad (1)$$

where $|\cdot|$ represents the magnitude, $\|\cdot\|_F$ is the Frobenius norm, and s and \hat{s} are the ground truth and predicted magnitude spectrograms, respectively. This loss focuses on the large magnitude components of the spectrograms.

The Log-Magnitude Loss is defined as:

$$\| \log(|STFT(s)| + \epsilon) - \log(|STFT(\hat{s})| + \epsilon) \|_1 \quad (2)$$

where ϵ is a small constant value added to prevent taking the logarithm of zero, and $\|\cdot\|_1$ is the $L1$ norm. This loss focuses on the small magnitude components of the spectrograms.

2.2 Diffusion

Inspired by the recent successes of diffusion models [Sohl-Dickstein et al. \(2015\)](#); [Ho et al. \(2020\)](#); [Kingma et al. \(2021\)](#) in solving audio tasks [Rouard and Hadjeres \(2021\)](#); [Kong et al. \(2020\)](#), we chose to employ them for the task of synthesizing mel spectrograms. Diffusion models can be thought of as a Markovian Hierarchical Variational Autoencoder [Luo \(2022\)](#). They define a markov chain of steps to slowly add random noise to the data and then learn the reverse process to synthesize data samples from noise.

2.2.1 Forward Process

Given a real data distribution $q(x_0)$, we draw a sample x_0 from the distribution, $x_0 \sim q(x)$. Then, we define a forward noising process $q(x_t|x_{t-1})$ that gradually adds Gaussian noise to the sample according to a predefined schedule $\beta_t \in (0, 1)_{t=1}^T$, where $\beta_1 < \beta_2 < \dots < \beta_T$. Specifically, the sample distribution at each time step is given by:

$$q(x_t|x_{t-1}) = \mathcal{N}(x_t; \sqrt{1 - \beta_t}x_{t-1}, \beta_t \mathbf{I}) \quad (3)$$

And the distribution over the entire sequence of samples $x_{1:T}$ given the initial sample x_0 is given by:

$$q(x_{1:T}|x_0) = \prod_{t=1}^T q(x_t|x_{t-1}) \quad (4)$$

As $T \rightarrow \infty$, the distribution of x_T approaches the standard Gaussian distribution.

To sample from the forward distribution, we can draw a sample x_t at each time step t from a conditional Gaussian with mean $\mu_t = \sqrt{1 - \beta_t}x_{t-1}$ and variance $\sigma^2 = \beta_t$ as follows:

$$x_t = \sqrt{1 - \beta_t}x_{t-1} + \sqrt{\beta_t}\epsilon \quad \text{where } \epsilon \sim \mathcal{N}(\mathbf{0}, \mathbf{I}) \quad (5)$$

The forward noising process in diffusion models has the property that, using the reparameterization trick, we can sample x_t at any arbitrary timestep. This property is described in [Song et al. \(2020\)](#); [Luo \(2022\)](#); [Weng \(2021\)](#). Let $\alpha_t = 1 - \beta_t$ and $\bar{\alpha}_t = \prod_{i=1}^t \alpha_i$. The process can be expressed as follows:

$$\begin{aligned} x_t &= \sqrt{\alpha_t}x_{t-1} + \sqrt{1 - \alpha_t}\epsilon_{t-1} \\ &= \sqrt{\alpha_t\alpha_{t-1}}x_{t-2} + \sqrt{1 - \alpha_t\alpha_{t-1}}\bar{\epsilon}_{t-2} \\ &= \dots \\ &= \sqrt{\alpha_t}x_0 + \sqrt{1 - \alpha_t}\epsilon \end{aligned} \quad (6)$$

where, $\epsilon_{t-1}, \epsilon_{t-2}, \dots \sim \mathcal{N}(\mathbf{0}, \mathbf{I})$. $\bar{\epsilon}_{t-2}$ is a combination of two Gaussian distributions with different variances, $\mathcal{N}(\mathbf{0}, \sigma_1^2 \mathbf{I})$ and $\mathcal{N}(\mathbf{0}, \sigma_2^2 \mathbf{I})$, such that:

$$\bar{\epsilon}_{t-2} = \sqrt{(1 - \alpha_t) + \alpha_t(1 - \alpha_{t-1})} = \sqrt{1 - \alpha_t\alpha_{t-1}} \quad (7)$$

2.2.2 Reverse Process

To generate a sample from a Gaussian noise input $x_T \sim \mathcal{N}(\mathbf{0}, \mathbf{I})$, we reverse the forward process by sampling from $q(x_{t-1}|x_t)$. However, $q(x_{t-1}|x_t)$ depends on the entire dataset, so we learn an approximate model p_θ :

$$p_\theta(\mathbf{x}_{t-1}|\mathbf{x}_t) = \mathcal{N}(\mathbf{x}_{t-1}; \mu_\theta(\mathbf{x}_t, t), \Sigma_\theta(\mathbf{x}_t, t)) \quad (8)$$

$$p_\theta(\mathbf{x}_{0:T}) = p(\mathbf{x}_T) \prod_{t=1}^T p_\theta(\mathbf{x}_{t-1}|\mathbf{x}_t) \quad (9)$$

The reverse conditional probability becomes tractable when it is conditioned on \mathbf{x}_0 :

$$q(\mathbf{x}_{t-1}|\mathbf{x}_t, \mathbf{x}_0) = \mathcal{N}(\mathbf{x}_{t-1}; \tilde{\mu}_t(\mathbf{x}_t, \mathbf{x}_0), \tilde{\Sigma}_t(\mathbf{x}_t, \mathbf{x}_0)) \quad (10)$$

Similar to [Ho et al. \(2020\)](#), we fix the variance to:

$$\Sigma_\theta(\mathbf{x}_t, \mathbf{x}_0) = \sigma_t^2 \mathbf{I} = \tilde{\beta}_t \mathbf{I} \quad (11)$$

and learn only the mean μ_θ . This gives us:

$$q(\mathbf{x}_{t-1}|\mathbf{x}_t, \mathbf{x}_0) = \mathcal{N}(\mathbf{x}_{t-1}; \tilde{\mu}_t(\mathbf{x}_t, \mathbf{x}_0), \tilde{\beta}_t \mathbf{I}) \quad (12)$$

Using Bayes' rule, we can derive the following equations:

$$\tilde{\mu}_t(\mathbf{x}_t, \mathbf{x}_0) = \frac{\sqrt{\alpha_t}(1 - \bar{\alpha}_{t-1})}{1 - \bar{\alpha}_t} \mathbf{x}_t + \frac{\sqrt{\bar{\alpha}_{t-1}\beta_t}}{1 - \bar{\alpha}_{t-1}} \mathbf{x}_0 \quad (13)$$

$$\tilde{\beta}_t = \frac{1 - \bar{\alpha}_{t-1}}{1 - \bar{\alpha}_t} \cdot \beta_t \quad (14)$$

By substituting $\mathbf{x}_0 = \frac{1}{\sqrt{\bar{\alpha}_t}}(\mathbf{x}_t - \sqrt{1 - \bar{\alpha}_t}\epsilon_t)$ into the above equation for $\tilde{\mu}_t(\mathbf{x}_t, \mathbf{x}_0)$, we get:

$$\tilde{\mu}_t(\mathbf{x}_t, \mathbf{x}_0) = \frac{1}{\sqrt{\bar{\alpha}_t}}(\mathbf{x}_t - \frac{1 - \alpha_t}{\sqrt{1 - \bar{\alpha}_t}}\epsilon_t) \quad (15)$$

This equation allows us to compute the mean of the distribution $q(\mathbf{x}_{t-1}|\mathbf{x}_t, \mathbf{x}_0)$ given \mathbf{x}_t and \mathbf{x}_0 . The variance of this distribution is fixed to $\tilde{\beta}_t \mathbf{I}$, where $\tilde{\beta}_t$ is given by the equation $\tilde{\beta}_t = \frac{1 - \bar{\alpha}_{t-1}}{1 - \bar{\alpha}_t} \cdot \beta_t$. We can then sample from this distribution to obtain a sample of \mathbf{x}_{t-1} given \mathbf{x}_t and \mathbf{x}_0 . This process can be repeated to generate samples of $\mathbf{x}_{t-2}, \mathbf{x}_{t-3}, \dots, \mathbf{x}_0$ given \mathbf{x}_T .

2.2.3 Loss Function

As \mathbf{x}_t is available during training, we can use it to reparameterize the Gaussian mean term and predict ϵ_t given \mathbf{x}_t and t . This is done with the following equation:

$$\tilde{\mu}_t(\mathbf{x}_t, \mathbf{x}_0) = \frac{1}{\sqrt{\bar{\alpha}_t}}(\mathbf{x}_t - \frac{1 - \alpha_t}{\sqrt{1 - \bar{\alpha}_t}}\epsilon_\theta(\mathbf{x}_t, t)) \quad (16)$$

We then use the simplified loss term as described by [Ho et al. \(2020\)](#). Resulting in the following equations:

$$\begin{aligned} L_t &= \mathbb{E}_{t \sim [1, T], \mathbf{x}_0, \epsilon_t} [\|\epsilon_t - \epsilon_\theta(\mathbf{x}_t, t)\|_2^2] \\ &= \mathbb{E}_{t \sim [1, T], \mathbf{x}_0, \epsilon_t} [\|\epsilon_t - \epsilon_\theta(\sqrt{\alpha_t}\mathbf{x}_0 + \sqrt{1 - \alpha_t}\epsilon_t, t)\|_2^2] \end{aligned} \quad (17)$$

3 Architecture

Motivated by the success of the patch embedding tokenization scheme in the Vision Transformer (ViT) [Dosovitskiy et al. \(2020\)](#), we propose a similar tokenization scheme for audio based on mel spectrograms. Specifically, we view mel spectrograms as a sequence of tokens, where the sequence length is equal to the time frames and the dimensionality of each token is equal to the number of mel frequencies. This is similar to taking a patch along the frequency dimension, with a patch size equal to the number of mel frequencies.

In contrast to other methods that treat mel spectrograms as images, our approach offers efficiency gains by reducing the context size. For a mel spectrogram with dimensions *channels* \times *frequencies* \times *time frames*, our context size is reduced to *channels* \times *time frames*. Furthermore, we process channels independently, allowing our method to be applicable to an arbitrary number of channels. These considerations have been incorporated into the design of our U-Net (see Section 3.1) and Neural Vocoder (see Section 3.2).

3.1 U-Net

U-Nets [Ronneberger et al. \(2015\)](#) are a popular choice for image segmentation tasks due to their ability to accurately model fine details and localize features through the use of skip connections. These neural networks have also been greatly applied to diffusion modeling [Nichol and Dhariwal \(2021\)](#); [Song et al. \(2020\)](#); [Ho et al. \(2020\)](#). In this work, we propose a U-Net architecture that combines the strengths of U-Nets with those of transformers [Vaswani et al. \(2017\)](#), which are known for their ability to capture long-range dependencies through self-attention mechanisms. The resulting model is able to capture both local and global context while remaining efficient (see Figure 1). We present components of the U-Net below.

3.1.1 Input and Output Layers

The input layer (tokenization layer) receives a 2D spectrogram $\mathbf{X} \in \mathbb{R}^{c \times f \times l}$, where c is the channel dimension (e.g., mono, stereo), f is the frequency dimension, and l is the time frames dimension. It reshapes and linearly projects it along the frequency dimension to obtain $\mathbf{H} \in \mathbb{R}^{d \times c \times t}$, where \mathbf{H} is the output, d is the frequency dimension after projection.

The output layer (detokenization layer) expects an input $\mathbf{H} \in \mathbb{R}^{d \times c \times t}$ and performs the inverse actions of the input layer, linearly projecting the input and reshaping it into $\mathbf{Y} \in \mathbb{R}^{c \times f \times l}$, where \mathbf{Y} is the output (see Figure 1).

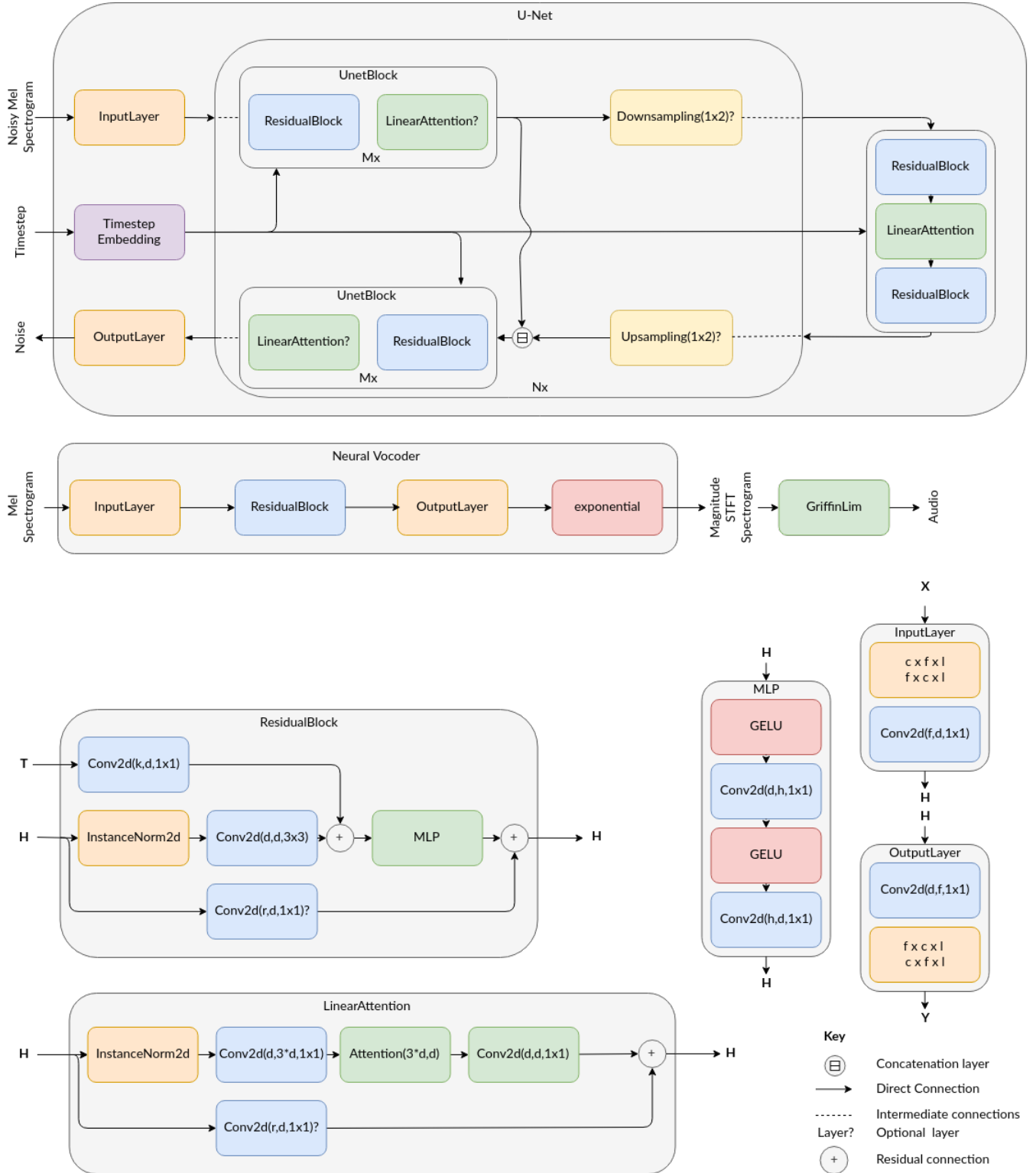


Figure 1: Proposed Msanii Architecture.

3.1.2 Residual Block

The input to our residual block is a 2D latent feature $\mathbf{H} \in \mathbb{R}^{d \times c \times l}$ and a timestep embedding feature $\mathbf{T} \in \mathbb{R}^{k \times 1 \times 1}$, where d is the frequency dimension, c is the channel dimension, l is the time frames dimension and k is the timestep. We first apply a pre-normalization layer to the input features, then perform a 3×3 padded convolution without changing the number of features to ensure that the input and output features have the same dimensions. While the U-Net is not sensitive to the specific type of normalization used, we have found that feature normalization performs better than weight normalization. This may be because the use of feature normalization forces the pre-activations to be Gaussian, resulting in output that is also Gaussian, which is useful for modeling noise that is typically Gaussian. We chose to use Instance Norm [Ulyanov et al. \(2016\)](#) in our implementation, as it has been observed to produce audio with fewer metallic artifacts in our Neural Vocoder [3.2](#).

After normalizing and projecting the input features, we project the timestep embedding features using a 1×1 convolution to match the feature dimensions of the latent features. We then sum the timestep embedding features and latent features and feed them into a Multi-Layer Perceptron (MLP). Our MLP is based on ConvNext [Liu et al. \(2022b\)](#) with a minor modification: we apply the GELU non-linearity before the first convolution layer. Finally, we apply the residual connection to the outputs of the MLP, and optionally project the residual features to match the dimensions of the MLP outputs.

3.1.3 Linear Attention

The input to our linear attention block is a 2D latent feature tensor $\mathbf{H} \in \mathbb{R}^{d \times c \times l}$. We first apply Instance Normalization to the input tensor before performing the attention operations. While the choice of attention mechanism does not significantly affect the performance of the U-Net, we have found that Linear Attention [Katharopoulos et al. \(2020\)](#) performs well due to its linear computational complexity.

Unlike some transformers [Vaswani et al. \(2017\)](#); [Dosovitskiy et al. \(2020\)](#); [Katharopoulos et al. \(2020\)](#); [Liu et al. \(2022b\)](#), we have observed that placing the attention layer after the residual block leads to better global coherence. Therefore, we adopt the post-attention mechanism for all of our tasks. Note that the U-Net is not sensitive to the specific attention mechanism used, which may be due to the fact that attention layers are used in the deeper layers where the context size is already small enough for global context to be easily captured.

3.1.4 Downsampling and Upsampling Layers

For downsampling the input features, we use a single 1×3 convolution layer with a stride of 1×2 and padding of 0×1 . This effectively reduces the time dimension of the input features by a factor of 2 while preserving the other dimensions.

For upsampling, we use a single 1×4 transposed convolution layer with a stride of 1×2 and padding of 0×1 . This effectively increases the time dimension of the input features by a factor of 2 while preserving the other dimensions.

3.2 Neural Vocoder

Our neural vocoder design is inspired by ISTFTNet [Kaneko et al. \(2022\)](#) and features a simple structure. It takes in an input mel spectrogram $\mathbf{X} \in \mathbb{R}^{c \times f_m \times l}$, where f_m is the frequency dimension of the mel spectrogram, and passes it through an input layer (see Section 3.1.1). The mel spectrogram is then processed through a single residual block (see Section 3.1.2), without the timestep embedding features, and finally through an output layer (see Section 3.1.1). This produces an STFT spectrogram $\mathbf{Y} \in \mathbb{R}^{c \times f_s \times l}$, where f_s is the frequency dimension of the magnitude STFT spectrogram. After the output layer, we apply an exponential activation to transform the magnitude spectrogram from log-space to linear-space (see Figure 1).

4 Experiments

4.1 Dataset

The dataset used for this work is the POP909 dataset [Wang* et al. \(2020\)](#), which consists of 909 MIDI files of popular pop songs. We synthesize 44.1kHz, stereo audio from the MIDI files using FluidSynth [Newmarch \(2017\)](#).

4.2 Training Details

4.2.1 Data Preprocessing

To synthesize mel spectrograms from the raw audio, we use an STFT window size of 2048 with a hop size of 1024, and apply 128 mel filterbanks to the resulting mel spectrogram. Since diffusion models typically operate on data in the range $[-1, 1]$ and expect the data to be Gaussian, we propose learning data-specific preprocessing techniques such as moving average parameters for standard scaling (see Algorithm 1) and min-max scaling (see Section A for more details).

4.2.2 Model Training

For our U-Net model, we set the width to 256 and use 2 U-Net blocks per resolution before applying downsam-

pling/upsampling layers. This results in a total of 14 U-Net blocks in the encoder and decoder, yielding a model with 49.8 million parameters. We set the timestep dimensionality to 128 and train the model for 110,000 steps using the Adam optimizer with a linear warmup of 500 steps. The value of β_1 for the Adam optimizer is set to 0.5, and the learning rate is set to 0.0002. We also train an exponential moving average version of the U-Net. The audio is limited to a length of 8,387,584 samples (190 seconds), chosen so that the resulting spectrogram is divisible by the number of downsampling layers. We use a batch size of 4 and train the model on a single GPU with 16 GB of memory. The specific GPU used may vary depending on availability.

For the Neural Vocoder model, we set the width to 256 and use a single residual block between the input and output layers. This results in a model with 1.4 million parameters. We train the model for 40,000 steps using the Adam optimizer with a linear warmup of 500 steps. The value of β_1 for the Adam optimizer is set to 0.5, and the learning rate is set to 0.0002. The audio is limited to a length of 523,264 samples (11 seconds), chosen so that the resulting spectrogram is divisible by the number of downsampling layers. We use a batch size of 8 and train the model on a single GPU with 16 GB of memory. The specific GPU used may vary depending on availability.

Both of our models are trained using 16-bit floating point precision.

For diffusion, we use the diffusers library [von Platen et al. \(2022\)](#) implementation of the DDIM algorithm [Song et al. \(2020\)](#) with 1000 timesteps and the cosine noise schedule from [Glide Nichol et al. \(2021\)](#) (see Section B for more details).

4.3 Evaluation

Our model is currently under active development, so we have performed manual evaluation of the samples. In this evaluation, we have focused on the long-term coherence and harmony of the generated samples. We have randomly generated samples with different seeds, rather than cherry-picking specific samples. However, we have not yet implemented any quantitative metrics for evaluating the performance of the model.

5 Results

5.1 Sampling

To evaluate the quality of the generated samples, we use subjective evaluations by human listeners. We generate

our samples using 200 steps of DDIM and 200 iterations of GriffinLim.

Overall, we observe that the generated samples have good long-term coherence, with the ability to maintain coherence for approximately 3 minutes. The samples also display diverse structures, including repeating patterns throughout the entire song. However, the generated samples do exhibit some degradation in quality compared to human-generated music, particularly in terms of realism and naturalness. This may be due in part to the use of GriffinLim for phase reconstruction.

One particularly notable strength of the generated samples is their diversity, despite being trained on a relatively small dataset. This suggests that the model is able to learn generalizable patterns from the training data.

We also observe that the model struggles with global coherence early on in training, and that the loss does not show significant improvement as training progresses. However, we do notice that with longer training, the model is able to achieve better global coherence and overall sample quality improves.

We do not observe any significant improvements by increasing the number of DDIM sampling steps. This suggests that training the model with a shorter noise schedule may lead to faster sampling. Further experimentation will be necessary to confirm this possibility.

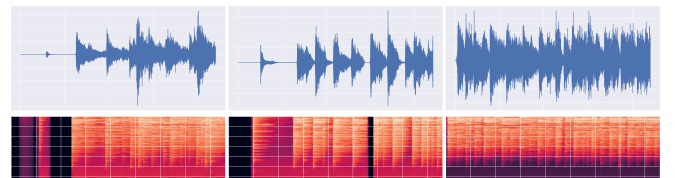


Figure 2: Illustrated from left to right are generated samples generated with 200 DDIM steps and 200 GriffinLim steps.

5.2 Audio-to-Audio (Style Transfer)

Starting with a mel spectrogram x_0 , we use Equation (6) to add noise at a desired timestep t , resulting in a noised mel spectrogram x_t . We then employ the reverse diffusion process (described in Subsection 2.2.2) to generate variations of the original audio that are more similar to our training data.

Our findings indicate that at low noise levels, the generated audio maintains the structure of the original audio while adapting the instruments and vocals to match those in the training data. However, the generated audio is too noisy at these low noise levels. On the other hand, when

the noise level is higher, the generated audio more closely resembles the training data, but the structure of the original audio is largely lost.

We also note that percussive sounds, such as drums, are less sensitive to increases in noise levels. Even at high noise levels, the overall structure of the generated audio is preserved.

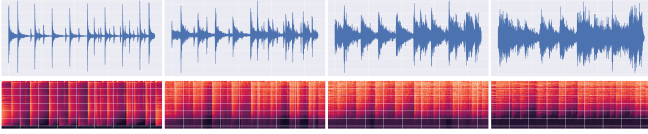


Figure 3: Illustrated, from left to right, are audio-to-audio samples of a drum loop with increasing noise timesteps, t : $t = 0$, $t = 100$, $t = 500$, and $t = 900$.

5.3 Interpolation

To perform audio interpolation using diffusion models, we start with two mel spectrograms x_0^1 and x_0^2 and use Equation (6) to add noise at the desired time step t , resulting in noised mel spectrograms x_t^1 and x_t^2 . We then interpolate the two noised spectrograms as follows: $x_t = \gamma x_t^1 + (1 - \gamma)x_t^2$, where $\gamma \in [0, 1]$ is the interpolation ratio. We apply the reverse diffusion process (described in Subsection 2.2.2) to generate interpolations of the two audio sources that are more similar to our training data.

We find that percussive sounds tend to be more prominent in the generated audio, even when the interpolation ratio is low. Similar to the results of the audio-to-audio task (see Subsection 5.2), we observe that at low noise levels the musical structure of the original audio is preserved, but the generated audio is noisy. On the other hand, at high noise levels, the musical structure of the generated audio closely resembles that of the training data.

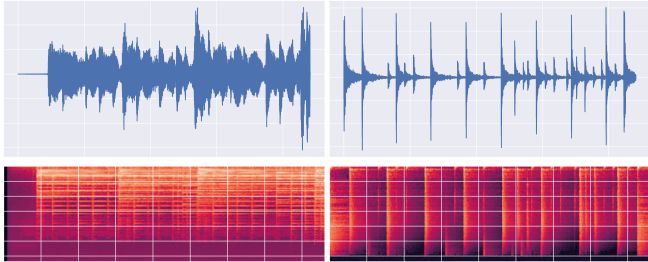


Figure 4: Original samples for interpolation, featuring a piano sample on the left and a drum loop on the right.

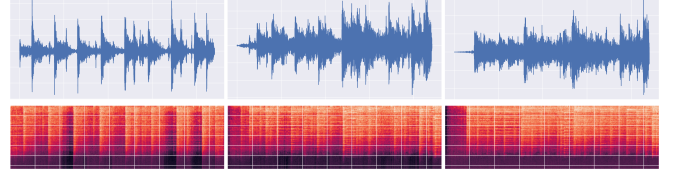


Figure 5: Illustrated, from left to right, are interpolation samples generated with a fixed noise timestep of $t = 200$ and varying ratios of the original samples: 0.1, 0.5, and 0.9 representing the proportion of the first original sample in each interpolated sample, respectively

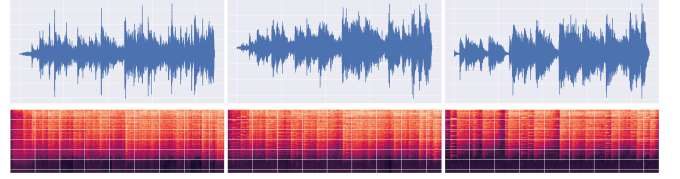


Figure 6: Illustrated, from left to right, are interpolation samples generated with a fixed ratio of 0.5 and increasing noise timesteps t : $t = 100$, $t = 500$, and $t = 900$, respectively.

5.4 Inpainting

In inpainting, we use a binary mask to identify the sections of an audio signal that should be kept and which should be removed. We then apply the Repaint algorithm [Lugmayr et al. \(2022\)](#), as implemented by [von Platen et al. \(2022\)](#), to fill in the masked sections.

However, our results show that the inpainted sections often lack rhythm and do not accurately capture the melody and harmony of the original audio. The inpainted audio sounds like a completely novel sample and does not resemble the original audio at all. This leads to a sudden change in the musical structure of the song in the inpainted sections.

We are not sure why this issue occurs. Further experimentation will be necessary to investigate and address this problem.

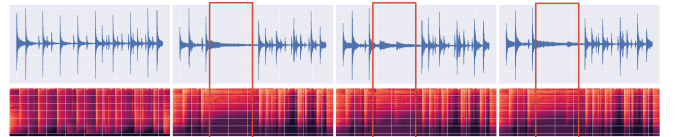


Figure 7: Illustrated from left to right: an original drum loop sample, and three inpainted versions generated using different seeds. The inpainted section in each sample is highlighted by the red box.

5.5 Outpainting

Outpainting involves extending the audio beyond the original recording by filling in additional sections with synthesized audio. To perform outpainting, we use the same algorithm as for inpainting (see Subsection 5.4). We take half of the original audio and concatenate it with an empty spectrogram, then specify a mask to inpaint the empty part.

Unfortunately, our results are sub-optimal. The outpainted sections often sound different from the original audio, often lacking rhythm. This is more pronounced because the different spans of audio that are outpainted result in regions of sudden change, making the audio sound like multiple different sources concatenated together.

We are not sure why this issue occurs. Further experimentation will be necessary to investigate and address this problem.

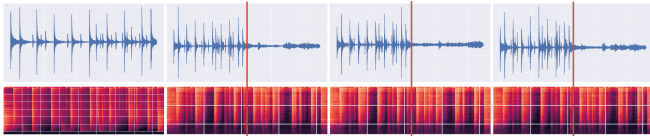


Figure 8: Illustrated from left to right: an original drum loop sample, and three outpainted versions generated using different seeds. The start of the outpainted section in each sample is highlighted by the red line.

6 Future Work

There are several directions in which this work could be extended to improve the quality and usefulness of the approach in a music production setting. Some potential avenues for future research include:

6.1 Conditional Generation

In this work, we have focused on unconditional generation, meaning that there is little to no control over the synthesized samples. However, in a music production setting, it is important to allow some control over the generated music. Possible approaches for adding controllability to the synthesis process include:

- Conditioning the model on factors such as lyrics, mood, or MIDI input. This could allow users to specify the content or style of the generated music.
- Allowing users to provide feedback during synthesis, either through explicit input or by interacting with the generated audio. This could allow users to shape the output in real-time or guide the synthesis process towards their desired results.

6.2 Evaluation in Realistic Settings

Our model has not yet been evaluated in a realistic setting, so it is important to determine its usefulness and effectiveness in music production. Possible approaches for evaluating the model include:

- Conducting user studies or case studies to assess the usefulness and effectiveness of the techniques in a music production setting. This could involve gathering feedback from music producers, musicians, or other industry professionals.
- Comparing the model’s output to that of human musicians or existing music production tools, using metrics such as subjective quality or task-specific performance. This could help to identify areas where the model excels or falls short compared to human or established standards.

6.3 Generalization to Other Audio Tasks

While this work has focused on music synthesis, we believe that the model could potentially be applied to other audio processing tasks as well. Some possible areas for exploration include:

- Classification tasks, such as genre classification or instrument recognition. This could help to determine the model’s ability to learn and represent musical concepts.
- Audio restoration tasks, such as noise reduction or audio enhancement. This could help to evaluate the model’s ability to manipulate and improve audio signals.

6.4 Improvements to Model Components

There are several ways in which the performance of the model and its components could be improved:

- Addressing the suboptimal performance of inpainting and outpainting for interactive audio design. This could involve redesigning the inpainting algorithm or incorporating new techniques for synthesizing audio.
- Scaling the model to improve its performance. This could help evaluate the scaling laws of the model.
- Incorporating new advancements in diffusion model sampling to allow for near real-time synthesis. This could help to make the model more responsive and interactive in a music production setting.

6.5 Expanding the Range of Generated Music

In this work, we have focused on generating music from a single instrument. However, there are many ways in which the model could be expanded to generate a wider range of music:

- Examining how the model handles more complex data with multiple instruments and vocals. This could allow the model to generate a wider range of musical styles and textures.
- Exploring the use of multi-track or stem generation, allowing users to have explicit control over each generated instrument. This could be particularly useful in a music production setting.
- Investigating the use of the model for generating music in different styles or genres, such as electronic, classical, or world music. This could help to assess the model’s ability to learn and represent diverse musical traditions.

Overall, there is significant potential for further research on our approach and its applications in the field of music synthesis AI, and we believe that these techniques have the potential to have a significant impact in the field.

7 Conclusion

In this work, we have introduced Msanii, a novel diffusion-based model for synthesizing long-context, high-fidelity music efficiently. By combining the expressiveness of mel spectrograms, the generative capabilities of diffusion models, and the vocoding capabilities of neural vocoders, Msanii is able to generate high quality audio. Our results demonstrate Msanii’s capabilities for generating minutes of coherent audio efficiently, and we have also discussed the potential for Msanii to be used in various applications in the field of music production. With its strong performance and versatility, we believe that Msanii has significant potential for further research and development. Overall, Msanii shows promise as a powerful tool for music synthesis and production.

8 Acknowledgement

We would like to express our gratitude to OpenAI for providing access to ChatGPT, which has been instrumental in revising our paper. The use of ChatGPT has greatly improved the clarity and readability of our work, and we are grateful for the assistance it has provided.

References

- Arik, S. Ö., Jun, H., and Diamos, G. (2018). Fast spectrogram inversion using multi-head convolutional neural networks. *IEEE Signal Processing Letters*, 26(1):94–98.
- Brown, T., Mann, B., Ryder, N., Subbiah, M., Kaplan, J. D., Dhariwal, P., Neelakantan, A., Shyam, P., Sastry, G., Askell, A., et al. (2020). Language models are few-shot learners. *Advances in neural information processing systems*, 33:1877–1901.
- Dhariwal, P., Jun, H., Payne, C., Kim, J. W., Radford, A., and Sutskever, I. (2020). Jukebox: A generative model for music. *arXiv preprint arXiv:2005.00341*.
- Dhariwal, P. and Nichol, A. (2021). Diffusion models beat gans on image synthesis. *Advances in Neural Information Processing Systems*, 34:8780–8794.
- Di Giorgi, B., Levy, M., and Sharp, R. (2022). Mel spectrogram inversion with stable pitch. *arXiv preprint arXiv:2208.12782*.
- Dieleman, S., van den Oord, A., and Simonyan, K. (2018). The challenge of realistic music generation: modelling raw audio at scale. *Advances in Neural Information Processing Systems*, 31.
- Dosovitskiy, A., Beyer, L., Kolesnikov, A., Weissenborn, D., Zhai, X., Unterthiner, T., Dehghani, M., Minderer, M., Heigold, G., Gelly, S., et al. (2020). An image is worth 16x16 words: Transformers for image recognition at scale. *arXiv preprint arXiv:2010.11929*.
- Engel, J., Agrawal, K. K., Chen, S., Gulrajani, I., Donahue, C., and Roberts, A. (2019). Gansynth: Adversarial neural audio synthesis. *arXiv preprint arXiv:1902.08710*.
- Goodfellow, I., Pouget-Abadie, J., Mirza, M., Xu, B., Warde-Farley, D., Ozair, S., Courville, A., and Bengio, Y. (2020). Generative adversarial networks. *Communications of the ACM*, 63(11):139–144.
- Griffin, D. and Lim, J. (1984). Signal estimation from modified short-time fourier transform. *IEEE Transactions on acoustics, speech, and signal processing*, 32(2):236–243.
- Ho, J., Jain, A., and Abbeel, P. (2020). Denoising diffusion probabilistic models. *Advances in Neural Information Processing Systems*, 33:6840–6851.
- Hwang, Y., Cho, H., Yang, H., Won, D.-O., Oh, I., and Lee, S.-W. (2020). Mel-spectrogram augmentation for sequence to sequence voice conversion. *arXiv preprint arXiv:2001.01401*.

- Kaneko, T., Tanaka, K., Kameoka, H., and Seki, S. (2022). Istftnet: Fast and lightweight mel-spectrogram vocoder incorporating inverse short-time fourier transform. In *ICASSP 2022-2022 IEEE International Conference on Acoustics, Speech and Signal Processing (ICASSP)*, pages 6207–6211. IEEE.
- Karras, T., Laine, S., Aittala, M., Hellsten, J., Lehtinen, J., and Aila, T. (2020). Analyzing and improving the image quality of stylegan. In *Proceedings of the IEEE/CVF conference on computer vision and pattern recognition*, pages 8110–8119.
- Katharopoulos, A., Vyas, A., Pappas, N., and Fleuret, F. (2020). Transformers are rnns: Fast autoregressive transformers with linear attention. In *International Conference on Machine Learning*, pages 5156–5165. PMLR.
- Kingma, D., Salimans, T., Poole, B., and Ho, J. (2021). Variational diffusion models. *Advances in neural information processing systems*, 34:21696–21707.
- Kingma, D. P. and Welling, M. (2013). Auto-encoding variational bayes. *arXiv preprint arXiv:1312.6114*.
- Kong, Z., Ping, W., Huang, J., Zhao, K., and Catanzaro, B. (2020). Diffwave: A versatile diffusion model for audio synthesis. *arXiv preprint arXiv:2009.09761*.
- Kumar, K., Kumar, R., de Boissiere, T., Gestin, L., Teoh, W. Z., Sotelo, J., de Brébisson, A., Bengio, Y., and Courville, A. C. (2019). Melgan: Generative adversarial networks for conditional waveform synthesis. *Advances in neural information processing systems*, 32.
- Liu, J., Li, C., Ren, Y., Chen, F., and Zhao, Z. (2022a). Diffsinger: Singing voice synthesis via shallow diffusion mechanism. In *Proceedings of the AAAI Conference on Artificial Intelligence*, volume 36, pages 11020–11028.
- Liu, Z., Mao, H., Wu, C.-Y., Feichtenhofer, C., Darrell, T., and Xie, S. (2022b). A convnet for the 2020s. In *Proceedings of the IEEE/CVF Conference on Computer Vision and Pattern Recognition*, pages 11976–11986.
- Lugmayr, A., Danelljan, M., Romero, A., Yu, F., Timofte, R., and Van Gool, L. (2022). Repaint: Inpainting using denoising diffusion probabilistic models. In *Proceedings of the IEEE/CVF Conference on Computer Vision and Pattern Recognition*, pages 11461–11471.
- Luo, C. (2022). Understanding diffusion models: A unified perspective. *arXiv preprint arXiv:2208.11970*.
- Marafioti, A., Perraudin, N., Holighaus, N., and Majdak, P. (2019). Adversarial generation of time-frequency features with application in audio synthesis. In *International conference on machine learning*, pages 4352–4362. PMLR.
- Newmarch, J. (2017). Fluidsynth. In *Linux Sound Programming*, pages 351–353. Springer.
- Nichol, A., Dhariwal, P., Ramesh, A., Shyam, P., Mishkin, P., McGrew, B., Sutskever, I., and Chen, M. (2021). Glide: Towards photorealistic image generation and editing with text-guided diffusion models. *arXiv preprint arXiv:2112.10741*.
- Nichol, A. Q. and Dhariwal, P. (2021). Improved denoising diffusion probabilistic models. In *International Conference on Machine Learning*, pages 8162–8171. PMLR.
- Pasini, M. and Schlüter, J. (2022). Musika! fast infinite waveform music generation. *arXiv preprint arXiv:2208.08706*.
- Perraudin, N., Balazs, P., and Søndergaard, P. L. (2013). A fast griffin-lim algorithm. In *2013 IEEE Workshop on Applications of Signal Processing to Audio and Acoustics*, pages 1–4. IEEE.
- Ramesh, A., Dhariwal, P., Nichol, A., Chu, C., and Chen, M. (2022). Hierarchical text-conditional image generation with clip latents. *arXiv preprint arXiv:2204.06125*.
- Rezende, D. and Mohamed, S. (2015). Variational inference with normalizing flows. In *International conference on machine learning*, pages 1530–1538. PMLR.
- Rombach, R., Blattmann, A., Lorenz, D., Esser, P., and Ommer, B. (2022). High-resolution image synthesis with latent diffusion models. In *Proceedings of the IEEE/CVF Conference on Computer Vision and Pattern Recognition*, pages 10684–10695.
- Ronneberger, O., Fischer, P., and Brox, T. (2015). U-net: Convolutional networks for biomedical image segmentation. In *International Conference on Medical image computing and computer-assisted intervention*, pages 234–241. Springer.
- Rouard, S. and Hadjeres, G. (2021). Crash: Raw audio score-based generative modeling for controllable high-resolution drum sound synthesis. *arXiv preprint arXiv:2106.07431*.
- Saharia, C., Chan, W., Saxena, S., Li, L., Whang, J., Denton, E., Ghasemipour, S. K. S., Ayan, B. K., Mahdavi, S. S., Lopes, R. G., et al. (2022). Photorealistic text-to-image diffusion models with deep language understanding. *arXiv preprint arXiv:2205.11487*.

- Scao, T. L., Fan, A., Akiki, C., Pavlick, E., Ilić, S., Hesslow, D., Castagné, R., Luccioni, A. S., Yvon, F., Gallé, M., et al. (2022). Bloom: A 176b-parameter open-access multilingual language model. *arXiv preprint arXiv:2211.05100*.
- Shen, J., Pang, R., Weiss, R. J., Schuster, M., Jaitly, N., Yang, Z., Chen, Z., Zhang, Y., Wang, Y., Skerry-Ryan, R., et al. (2017). Natural tts synthesis by conditioning wavenet on mel spectrogram predictions. arxiv e-prints. *arXiv preprint arXiv:1712.05884*.
- Sohl-Dickstein, J., Weiss, E., Maheswaranathan, N., and Ganguli, S. (2015). Deep unsupervised learning using nonequilibrium thermodynamics. In *International Conference on Machine Learning*, pages 2256–2265. PMLR.
- Song, J., Meng, C., and Ermon, S. (2020). Denoising diffusion implicit models. *arXiv preprint arXiv:2010.02502*.
- Ulyanov, D., Vedaldi, A., and Lempitsky, V. (2016). Instance normalization: The missing ingredient for fast stylization. *arXiv preprint arXiv:1607.08022*.
- Vasquez, S. and Lewis, M. (2019). Melnet: A generative model for audio in the frequency domain. *arXiv preprint arXiv:1906.01083*.
- Vaswani, A., Shazeer, N., Parmar, N., Uszkoreit, J., Jones, L., Gomez, A. N., Kaiser, Ł., and Polosukhin, I. (2017). Attention is all you need. *Advances in neural information processing systems*, 30.
- von Platen, P., Patil, S., Lozhkov, A., Cuenca, P., Lambert, N., Rasul, K., Davaadorj, M., and Wolf, T. (2022). Diffusers: State-of-the-art diffusion models. <https://github.com/huggingface/diffusers>.
- Wang*, Z., Chen*, K., Jiang, J., Zhang, Y., Xu, M., Dai, S., Bin, G., and Xia, G. (2020). Pop909: A pop-song dataset for music arrangement generation. In *Proceedings of 21st International Conference on Music Information Retrieval, ISMIR*.
- Weng, L. (2021). What are diffusion models? *lilian-weng.github.io*.

A Data Preprocessing

A.1 Standard Scaling (Normalization)

Algorithm 1 Standard Scaling Algorithm

Input: x : mini-Batch $B = \{x_{1\dots n}\}$, m : momentum, d : momentum decay, ϵ : epsilon

Output: $y = \frac{x - \mathbb{E}[x]}{\sqrt{\text{Var}[x] + \epsilon}}$

```

1: if no running statistics then
    # Initialize running statistics
2:    $\mu_R \leftarrow \frac{1}{n} \sum_{i=1}^n x_i$  # mean
3:    $\sigma_R^2 \leftarrow \frac{1}{n} \sum_{i=1}^n (x_i - \mu_R)^2$  # variance
4: end if

5: if in training mode then
    # Use mini-batch statistics
6:    $\mu_B \leftarrow \frac{1}{n} \sum_{i=1}^n x_i$  # mean
7:    $\sigma_B^2 \leftarrow \frac{1}{n} \sum_{i=1}^n (x_i - \mu_B)^2$  # variance

    # Update running statistics
8:    $m \leftarrow d \cdot m$  # momentum
9:    $\mu_R \leftarrow (1 - m) \cdot \mu_R + m \cdot \mu_B$  # mean
10:   $\sigma_R^2 \leftarrow (1 - m) \cdot \sigma_R^2 + m \cdot \sigma_B^2$  # variance
11: else
    # Use running statistics
12:   $\mu_B \leftarrow \mu_R$  # mean
13:   $\sigma_B^2 \leftarrow \sigma_R^2$  # variance
14: end if

15:  $y \leftarrow \frac{x - \mu_B}{\sqrt{\sigma_B^2 + \epsilon}}$ 

```

This algorithm standardizes the elements of the input x using the mean $\mathbb{E}[x]$ and variance $\text{Var}[x]$ of the input. The momentum m and momentum decay d are used to update the running statistics during training, and the small constant ϵ is used to prevent division by zero. If the model is in training mode, the batch statistics μ_B and σ_B^2 are used to compute the mean and variance. If the model is in inference mode, the running statistics μ_R and σ_R^2 are used instead.

A.2 Min-Max Scaling

Algorithm 2 Min-Max Scaling Algorithm

Input: x : mini-Batch $B = \{x_{1\dots n}\}$, y_{\min} : minimum value after scaling, y_{\max} : maximum value after scaling, m : momentum, d : momentum decay

Output: $y = \frac{x - \min(x)}{\max(x) - \min(x)} * (y_{\max} - y_{\min}) + y_{\min}$

```

1: if no running statistics then
    # Initialize running statistics
2:    $\min_R \leftarrow \min(x)$  # min
3:    $\max_R \leftarrow \max(x)$  # max
4: end if

5: if in training mode then
    # Use mini-batch statistics
6:    $\min_B \leftarrow \min(x)$  # min
7:    $\max_B \leftarrow \max(x)$  # max

    # Update running statistics
8:    $m \leftarrow d \cdot m$  # momentum
9:    $\min_R \leftarrow (1 - m) \cdot \min_R + m \cdot \min_B$  # min
10:   $\max_R \leftarrow (1 - m) \cdot \max_R + m \cdot \max_B$  # max
11: else
    # Use running statistics
12:   $\min_B \leftarrow \min_R$ 
13:   $\max_B \leftarrow \max_R$ 
14: end if

15:  $y = \frac{x - \min_B}{\max_B - \min_B} * (y_{\max} - y_{\min}) + y_{\min}$ 
16:  $y = \max(y_{\min}, \min(y, y_{\max}))$  # clamp  $y$  to be in the
    range  $[y_{\min}, y_{\max}]$ 

```

This algorithm scales the elements of the input x to be in the range $[y_{\min}, y_{\max}]$. The momentum m and momentum decay d are used to update the running statistics during training. If the model is in training mode, the batch statistics \min_B and \max_B are used to compute the min and max. If the model is in inference mode, the running statistics \min_R and \max_R are used instead.

B Hyper-parameters**B.1 Neural Vocoder**

Hyper-parameter	Value
Data	
Sample rate	44100
Audio length	523264
Audio channels	2
Batch size	8
Transforms	
FFT size	2048
Window length	2048
Hop length	1024
Mel frequencies	128
Feature scaling momentum	0.001
Feature scaling decay	0.99
GriffinLim iterations	200
Vocoder	
Model dimension	256
MLP hidden dimension factor	4
Training	
Learning rate (lr)	0.0002
Optimizer	Adam
Adam betas	0.5, 0.999
lr warmup iterations	500
lr warmup start factor	$\frac{1}{3}$
Precision	16
Training steps	40000

Table 1: Neural Vocoder hyper-parameters.

B.2 U-Net

Hyper-parameter	Value
Data	
Sample rate	44100
Audio Length	8387584
Audio channels	2
Batch size	4
Diffusion	
Noise schedule	cosine
Number of training timesteps	1000
Number of sampling steps	200
U-Net	
Base model dimension	256
Timestep dimension	128
MLP hidden dimension factor	4
Number of attention heads	8
Dimensionality factor	1,1,1,1,1,1
Dilations	1,1,1,1,1,1
Has attention	F, F, F, F, F, T, T
Has resampling	T, T, T, T, T, T, F
Blocks per resolution	2,2,2,2,2,2
EMA U-Net	
Start step	2000
Decay	0.995
Update every n-steps	10
Training	
Learning rate (lr)	0.0002
Optimizer	Adam
Adam betas	0.5, 0.999
lr warmup iterations	500
lr warmup start factor	$\frac{1}{3}$
Precision	16
Training steps	110000

Table 2: U-Net hyper-parameters.

C Optimizing U-Net Width for Improved Performance

The U-Net architecture, similar to transformers, can achieve significant performance gains by increasing its width. However, it is essential to consider the relationship between the width of the U-Net and the dimension of the spectrogram frequencies when using it as a feature.

For instance, using a U-Net with a width that is lower than the frequency dimension of the spectrogram forces the input layer to only learn the principal components of the mel spectrogram. This approach may work well for a clean mel spectrogram but is not suitable when the mel spectrogram is corrupted with noise.

Our experimentation has shown that it is crucial for the U-Net width to be at least 2x larger than the frequency dimension of the spectrogram to ensure optimal performance. Further experimentation is required to fully understand this phenomenon and to optimize the U-Net's width for improved performance.